

# Simulated Relationships between Sea Surface Temperatures and Tropical Convection in Climate Models and Their Implications for Tropical Cyclone Activity

JENNI L. EVANS AND JEFFREY J. WATERS

*Department of Meteorology, The Pennsylvania State University, University Park, Pennsylvania*

(Manuscript received 12 July 2011, in final form 25 May 2012)

## ABSTRACT

The impact of enhanced atmospheric CO<sub>2</sub> concentrations on tropical convection and sea surface temperatures (SSTs) over the global tropics is assessed using five fully coupled atmospheric–oceanic general circulation models (AOGCMs). Relationships between SST and either outgoing longwave radiation or convective precipitation rates are evaluated for three climate states: present day, a doubled-CO<sub>2</sub> scenario, and a quadrupled-CO<sub>2</sub> scenario. All AOGCMs capture a relationship between present-day outgoing longwave radiation (OLR) and SST and between convective precipitation rate (PRC) and SST: deep tropical convection (DTC)—signified by rapidly decreasing OLR and rapidly increasing PRC rates—occurs above an SST threshold of around 25°C. Consistent across all AOGCMs, as concentrations increase to 2 × CO<sub>2</sub> and 4 × CO<sub>2</sub>, the threshold SSTs for DTC to occur shift to 25.5°–28°C and 26.5°–30°C, respectively. Annual PRC rates in the 20°N–20°S region increase for two AOGCMs [Meteorological Research Institute Coupled General Circulation Model, version 2.3.2 (MRI CGCM2.3.2) and ECHAM5/Max Planck Institute Ocean Model (MPI-OM)] with increasing CO<sub>2</sub>, but PRC in the other three AOGCMs [Geophysical Fluid Dynamics Laboratory Climate Model versions 2.0 and 2.1 (GFDL CM2.0 and CM2.1) and National Center for Atmospheric Research (NCAR) Parallel Climate Model (PCM)] exhibits almost no change. Within this tropical zone, increased CO<sub>2</sub> concentrations yield up to a 6.1% increase in the number of locations with monthly averaged PRC exceeding two established DTC thresholds (12 and 14 mm day<sup>-1</sup>). These results indicate that, although the SST threshold for DTC is projected to shift with increasing atmospheric CO<sub>2</sub> concentrations, there will not be an expansion of regions experiencing DTC. One implication of these findings is that there will be little change in regions experiencing tropical cyclogenesis in future climate states.

## 1. Introduction

Organization of tropical convection varies greatly across spatial and temporal scales. Mesoscale convective systems (MCSs) and tropical cyclones (TCs) produce sustained, intense rainfall over the lifetime of the respective system; the system lifetime increases with increasing system organization from hours (MCSs) to days, or even weeks for TCs. Further, increased convective system organization leads to increased rainfall rates, with the greatest intensity being associated with TCs (e.g., Shemo and Evans 1996). MCSs have typical lifetimes of only 6–18 h, but occur so frequently throughout the tropics that they are a dominant contributor to

the annual tropical rainfall (e.g., Shemo and Evans 1996), while rainfall associated with TCs produces more extreme rain events on regional scales such as the tropical North Atlantic (Lau et al. 2008). Combined, these types of organized convective systems have been shown to be the dominant source of annual rainfall throughout much of the tropics (Evans and Jaskiewicz 2001).

Malkus (1963) describes the cooperative role of deep tropical convection (DTC) in driving the main “firebox” of the atmospheric heat engine, the Hadley circulation. She notes that these tropical convective “hot towers” are a vital link between the tropical and subtropical moisture and radiation budgets and relates development of DTC to tropical sea surface temperatures (SSTs). Many subsequent investigations have supported these insights into the links between tropical convection, radiation, SST, and the Hadley circulation (e.g., Graham and Barnett 1987; Lau et al. 1997; Dutton et al. 2000; Evans and Jaskiewicz 2001; Fierro et al. 2009). Because

---

*Corresponding author address:* Jenni L. Evans, Dept. of Meteorology, The Pennsylvania State University, 503 Walker Bldg., University Park, PA 16802.  
E-mail: evans@meteo.psu.edu

perturbations in DTC may have a profound impact on the general circulation (e.g., Oort and Yienger 1996), it is essential to understand the potential changes in tropical convection caused by increases in atmospheric carbon dioxide ( $\text{CO}_2$ ) concentrations.

Low values of outgoing longwave radiation (OLR) at the top of the atmosphere correspond to the very cold cloud tops of deep tropical convection, while similar OLR in the midlatitudes likely represents stratiform clouds; OLR values less than  $240 \text{ W m}^{-2}$  are commonly used to signify DTC (e.g., Lau et al. 1997). Many investigators have linked the incidence of DTC to underlying areas of warm SST (e.g., Graham and Barnett 1987; Zhang 1993; Dutton et al. 2000; Folkins and Braun 2003; Webster and Evans 2012, manuscript submitted to *Geophys. Res. Lett.*, hereafter WE). Lau et al. (1997) identify a threshold temperature for DTC: they observed a sharp increase in cloud-top height (decrease in OLR) for a threshold SST between  $25.5^\circ$  and  $28^\circ\text{C}$ . Consistent with Graham and Barnett (1987), Lau et al. (1997) attribute the range of threshold SSTs to modulation of the convection by the large-scale flow. Folkins and Braun (2003) identify the threshold SST range to be between  $26^\circ$  and  $29^\circ\text{C}$ ; they relate this threshold to an increase in the mass flux out of the boundary layer to drive a more vigorous convection. The rapid increase in tropical rainfall for this SST range has been reported by many investigators (e.g., Gadgil et al. 1984; Zhang 1993; Evans and Shemo 1996). Above this range, tropical rainfall rates drop considerably due to a local balance between the low equivalent potential temperature ( $\theta_e$ ) air being transported into the convective boundary layer via convective downdrafts, and high  $\theta_e$  near-surface air being transferred into the boundary layer via the deep convective source near the surface (Graham and Barnett 1987). Such a balance in the surface heat budget reduces the boundary layer latent heat flux, thereby suppressing convective activity. Dutton et al. (2000) examined the impact of enhanced atmospheric  $\text{CO}_2$  concentrations on the SST–tropical convection relationship using the coupled National Center for Atmospheric Research Climate System Model, version 1 (NCAR CSM1). They found that the simulated threshold temperature for tropical convection increased as  $\text{CO}_2$  concentrations (and tropical SST) increased, a result that is also supported by Williams et al. (2009). Furthermore, although annual tropical precipitation rates increased somewhat, Dutton et al. (2000) did not diagnose any expansion in the regions of DTC even for warming corresponding to concentrations of  $4 \times \text{CO}_2$ . Trenberth (2011) also found that increased SSTs in future climates would have little effect on annual precipitation in regions such as the tropics, but proposed that regions currently experiencing

DTC would experience more intense rainfall events. On the other hand, Gualdi et al. (2008) suggest that the increase in tropically averaged precipitation with increasing  $\text{CO}_2$  concentrations would be accompanied by a reduction in convective activity due to an increase in static stability. In their study of the South Asian summer monsoon response to anthropogenic climate change, Fan et al. (2012) diagnosed a trend toward increased precipitation rates in the warmer climate regime accompanied by increased static stability and a weaker monsoon circulation in the majority of the AOGCM analyzed.

SST and DTC also have important implications for tropical cyclogenesis (TCG) and TC intensity, so any systematic modifications of SST or DTC in future climates should be expected to impact TC characteristics. Gray (1968, 1979) recognized that TCs most commonly develop in regions where, among other precursors, SSTs are at least  $26^\circ\text{C}$ . Several studies have found that the areal extent of DTC remains consistent as atmospheric  $\text{CO}_2$  concentrations and surface temperatures rise, suggesting little change in the areal extent of TCG (Dutton et al. 2000; Walsh 2004; Gualdi et al. 2008). Next, there is a common acceptance that a relationship exists between increasing SST and TC rainfall intensity (Evans et al. 1994). Increasing SST leads to an increase in potential evaporation near the surface, thereby enhancing convective activity to drive intensification. Theories for TC potential intensity support the likelihood that increases in global surface temperatures may lead to an increase in TC maximum intensity (e.g., Emanuel 1995), with enhanced peak precipitation rates also diagnosed for a small percentage of simulated TCs (Walsh 2004; Gualdi et al. 2008). These results suggest that future climate states with increased SSTs may cause stronger TCs with higher rain rates to develop over the same regions. However, theoretical potential intensities are almost never observed (e.g., Evans 1993) and no observed trend in TC intensity is evident above a  $\sim 28^\circ\text{C}$  SST threshold (remarkably similar to the deep convection threshold discussed above) (Evans 1993; Emanuel 2000).

Some researchers have evaluated how well atmosphere–ocean general circulation models (AOGCMs) and GCMs forecast TCG activity in enhanced  $\text{CO}_2$  environments using widely accepted seasonal TCG parameters that are derived from large-scale environmental fields [such as the seasonal genesis parameter of Gray (1968)]. The resulting yearly genesis fields in future climate states implied significant increases in TC frequency (Ryan et al. 1992; Royer et al. 1998; Druyen et al. 1999). In many cases, the results were driven by simulated changes in the ocean thermal energy term and the vertical equivalent potential temperature gradients in the tropics. These results are confirmed in the more recent study of Waters et al. (2012).

TABLE 1. AOGCM name and resolution, modeling center, initial and maximum CO<sub>2</sub> concentrations, and the model 10-yr bands in which threshold CO<sub>2</sub> concentrations of 355, 710, and 1144–1416 ppmv were reached (Randall et al. 2007). Additional background information on these simulations was obtained from PCMDI (2010). For the remainder of this paper, we will refer to these concentrations as 1 × CO<sub>2</sub>, 2 × CO<sub>2</sub>, and 4 × CO<sub>2</sub> respectively.

AOGCM (resolution)	Modeling organization and model data reference	Initial/max CO <sub>2</sub> concentration (ppmv)	Model 10-yr band for given concentration (ppmv)		
			355	710	4 × CO <sub>2</sub>
GFDL CM2.0 (~2.0° × 2.5°/L24)	GFDL (2010a)	286/1144	22–31	91–100	140–149
GFDL CM2.1 (~2.0° × 2.5°/L24)	GFDL (2010b) (semi-Lagrangian)	286/1144	22–31	91–100	140–149
ECHAM5/MPI-OM (~1.9° × 1.9, T63/L)	Max Planck Institute (Roeckner 2010)	286/1144	22–31	91–100	140–149
MRI-CGCM2.3.2 (~2.8° × 2.8°, T42/L30)	MRI (2010a,b)	348/1392	2–11	72–81	140–149
NCAR PCM (~2.8° × 2.8°, T42/L26)	NCAR (2010)	354/1416	1–10	70–79	140–149

Other studies have focused more on TC intensity and size in future climate states. For example, Bengtsson et al. (2007) and Oouchi et al. (2006) suggest that a markedly warmer climate may lead to an increase in TC intensity but a decrease in TC size; an overall reduction in the global number of TCs is simulated, but changes vary by region. In the projected climate state, an increase in static stability causes convection to follow a less steep lapse rate in a warmer and moister climate. Furthermore, the increase in temperature and atmospheric water vapor content (longer residence time of water in the atmosphere, which weakens tropical circulation) provides more energy for the storms so that when they do occur, these components contribute toward a more intense storm. Likewise, Emanuel et al. (2008) produce synthetic TCs in five ocean basins using output spanning two time periods (1981–2000 and 2181–00) from seven GCMs. As with the previous two studies, Emanuel et al. (2008) conclude that global warming should reduce the global frequency of TCs, but these frequency shifts will vary by region and their intensities may increase in some locations. Such findings have also been supported by Sugi et al. (2009), who suggest that regional change in TC frequency is strongly affected by changes in tropical circulation, SST, and convective activity.

The purpose of this study is to document the relationship between DTC and SST over the global tropics and subtropics as simulated by five fully coupled AOGCMs (Table 1) from the most recent Intergovernmental Panel on Climate Change (IPCC) Fourth Assessment Report (AR4) (Randall et al. 2007). In particular, we revisit the question of the impact of enhanced atmospheric CO<sub>2</sub> concentrations on DTC and its relationship to SST. Using these evaluations, our main goal is to infer changes in convective support for tropical cyclones in an evolving background climate and to explore how the SST–tropical convection relationship in enhanced CO<sub>2</sub> conditions differs from present conditions. Details of the AOGCMs used and the analysis methodology applied are provided

in section 2, assessments of the AOGCMs' skill at replicating the observed relationships between deep convection and SST and the results of comparisons between current and possible future climate states are discussed in section 3, and these results are summarized and couched in a broader context in section 4.

## 2. Method

Variations in DTC and SST and the interrelationships between them are investigated for five IPCC AR4 AOGCM experiments driven by the transient 1PCTTO4X scenario (information online at [http://www.ipcc-data.org/sres/ddc\\_sres\\_emissions.html#1pto4x](http://www.ipcc-data.org/sres/ddc_sres_emissions.html#1pto4x)) (Table 1; Randall et al. 2007). Under this scenario, atmospheric CO<sub>2</sub> concentrations increase 1% yr<sup>-1</sup> until initial concentrations quadruple and then are held fixed.

Our analyses focus on variations in the monthly values of the top-of-the-atmosphere outgoing radiative flux (OLR in W m<sup>-2</sup>), open-ocean SST (°C), and convective precipitation rate (PRC in mm day<sup>-1</sup>). Either land fraction or surface altitude is used (depending on the AOGCM) to exclude grid points that intrude over land. We focus on three threshold concentration levels: 1 × CO<sub>2</sub> (taken as 355 ppmv), 2 × CO<sub>2</sub> (710 ppmv), and 4 × CO<sub>2</sub> (when the initial CO<sub>2</sub> concentration for each AOGCM reaches 4 times its initial value<sup>1</sup>) (Table 1). The decade beginning at each of these years was analyzed for all AOGCMs at each CO<sub>2</sub> threshold.

<sup>1</sup> The final CO<sub>2</sub> concentration for each AOGCM was 4 times its initial value, and since the models began with varied CO<sub>2</sub> concentrations but increased at 1% yr<sup>-1</sup>, “quadruple CO<sub>2</sub>” occurred in all cases at simulation year 140 and spanned the range 1144–1416 ppmv for the AOGCMs examined here (Table 1). The choice of “standard” values for the analyses at 1 × CO<sub>2</sub> and 2 × CO<sub>2</sub> concentrations allows for direct comparison with Dutton et al. (2000). Use of the individual model 4 × CO<sub>2</sub> concentrations captures the most extreme forcing for each model simulation examined.

TABLE 2. SST averaged over the band 40°N–40°S for each 10-yr band of the three CO<sub>2</sub> concentrations analyzed and SST change ( $4 \times \text{CO}_2 - 1 \times \text{CO}_2$ ).

AOGCM	1 × CO <sub>2</sub>	2 × CO <sub>2</sub>	4 × CO <sub>2</sub>	Increase (°C) (4 × CO <sub>2</sub> – 1 × CO <sub>2</sub> )
GFDL CM2.0	23.1	24.5	25.6	2.5
GFDL CM2.1	23.4	24.7	25.9	2.5
ECHAM5/MPI-OM	24.7	26.8	28.7	4.0
MRI-CGCM2.3.2	24.2	25.9	27.4	3.2
NCAR PCM	23.8	24.7	25.9	2.1

A variety of AOGCM fields are considered as proxies for DTC, but we report here on OLR and the convective precipitation rate, PRC. We analyze the relationships between monthly averaged OLR and SST (OLR/SST) and between monthly averaged PRC and SST (PRC/SST) over the latitude band 40°N–40°S for the three representative CO<sub>2</sub> concentrations (Tables 2 and 3).

Evolution of the relationship between collocated values of monthly averaged OLR and SST across the three atmospheric CO<sub>2</sub> doubling scenarios for each of the five AOGCMs is analyzed (Figs. 2 and 3). We compare changes in these distributions to the SST averaged over 40°N–40°S for each AOGCM and for each successive CO<sub>2</sub>-doubling scenario (Table 2). We repeat this process for PRC and SST across each CO<sub>2</sub>-doubling scenario (Figs. 4 and 5). OLR and PRC from each AOGCM are binned by SST in 0.5°C increments from 10° to 40°C (Figs. 3 and 5). If any bin lacks data, the average OLR and PRC values are set to zero. Note that for this analysis (Figs. 2–5), we produce results at the grid resolution of the models (as opposed to interpolating data over a common grid) as a method to capture differences in model response due to resolution and the genuine features of each model.

Annual precipitation rates over the tropical oceans (20°N–20°S) most strongly influence the monthly and annually averaged precipitation rates for the larger tropical and subtropical region (40°N–40°S; Fig. 6). We use three different analyses to examine the response of convection to enhanced atmospheric CO<sub>2</sub>. In the first approach, which is based on a similar method described in Dutton et al. (2000), we calculate annually averaged tropical precipitation rates across the 20°N–20°S tropical zone (Table 3). In the second approach, time series of spatially averaged annual precipitation rates are computed, then normalized by the full 140-yr (model years 1–140) average (Fig. 7, Table 3). In the third and final method, the spatial extent of high tropical precipitation rates is explored: the number of model ocean grid points with monthly averaged tropical precipitation rates exceeding 12 and 14 mm day<sup>-1</sup> is computed relative to the total number of grid points in the domain (Figs. 8a and 8b, Table 4).

### 3. Results

We analyze a set of AOGCMs selected to exclude model outliers while capturing a sufficient range of climate sensitivity in the IPCC simulations. Climate sensitivity metrics characterize the response of the global climate system to a given atmospheric, oceanic, or radiative forcing. The magnitude of the sensitivity is determined by the combination of internal positive and negative feedbacks in response to the applied forcing. Two sensitivity metrics are commonly used: the equilibrium climate sensitivity (ECS) and the transient climate sensitivity (TCS). ECS is calculated from the global annual mean surface temperature change resulting after the climate system has reached a new equilibrium in response to a doubling of CO<sub>2</sub>. TCS is the difference in the global annual mean surface air temperature change averaged over a 20-yr period centered at the time of CO<sub>2</sub> doubling. Making use of the ECS and TCS, we see that the National Center for Atmospheric Research (NCAR) Parallel Climate Model (PCM) AOGCM exhibits the lowest climate sensitivity by either measure (Table 5) while the ECHAM5/Max Planck Institute Ocean Model (MPI-OM) and Meteorological Research Institute Coupled General Circulation Model, version 2.3.2 (MRI CGCM2.3.2), have the highest climate sensitivities of the AOGCMs analyzed here and are near the top of the TCS range for the full set of IPCC AR4 models (Randall et al. 2007). Thus, this subset of AOGCMs provides a varied set of

TABLE 3. Annual PRCs averaged over the band 20°N–20°S during the first and last 10-yr periods of each AOGCM simulation and their respective differences.

AOGCM	PRC (mm day <sup>-1</sup> )			
	Years 1–10	Years 131–140	Change	Change (%)
GFDL CM2.0	3.89	4.01	+0.12	3.1
GFDL CM2.1	4.29	4.33	+0.04	0.9
ECHAM5/MPI-OM	4.27	4.83	+0.56	13.1
MRI-CGCM2.3.2	3.52	3.97	+0.45	12.8
NCAR PCM	4.90	5.08	+0.18	3.7

TABLE 4. Percentage of model ocean grid points per month exceeding 12 and 14 mm day<sup>-1</sup> thresholds in the band 20°N–20°S.

AOGCM	Percentage of model ocean grid points 20°N–20°S > 12 mm day <sup>-1</sup>			Percentage of model ocean grid points 20°N–20°S > 14 mm day <sup>-1</sup>		
	Years 1–10	Years 131–140	Change	Years 1–10	Years 131–140	Change
GFDL CM2.0	8.71	9.66	+0.95	5.58	6.20	+0.62
GFDL CM2.1	9.31	10.04	+0.73	5.75	6.24	+0.49
ECHAM5/MPI-OM	8.25	14.37	+6.12	4.22	9.43	+5.21
MRI-CGCM2.3.2	5.15	7.43	+2.28	2.75	4.28	+1.53
NCAR PCM	12.02	13.61	+1.59	8.25	9.52	+1.27

scenarios for exploring the response of the convective tropics to global climate change.

SST changes for increased levels of CO<sub>2</sub> averaged over all oceanic locations in the band 40°N–40°S (Table 2) track these climate sensitivities: the AOGCM with the largest ECS and TCS—the ECHAM5/MPI-OM—yields the largest SST increase (4.0°C) and the least sensitive AOGCM—the NCAR PCM—yields the lowest SST increase (2.1°C); SST changes for the remaining AOGCMs in the set lie within this range (Table 2). Changes in the globally averaged surface temperature (based on weighted area averages of each grid cell) with CO<sub>2</sub> increase are substantially larger than the tropical SST (or average tropical surface temperature) changes (Tables 2 and 6). Inspection of the spread in globally averaged surface temperature between the initial and final CO<sub>2</sub> concentrations (Fig. 1, Table 6) is revealing. The globally averaged surface temperature increase across the AOGCMs analyzed here ranges from 2.8° to 4.9°C, a substantial proportion of the variance in the complete set of IPCC4 AOGCMs (1.1°–6.4°C; additional information online at <http://www.epa.gov/climatechange/science/futurec.html#projections>).

#### a. OLR versus SST (40°N–40°S)

Relationships between SST and the two metrics of tropical convection intensity used here (OLR and PRC) are examined across this set of AOGCMs for the selected CO<sub>2</sub> thresholds. There is a noticeable association between increased atmospheric CO<sub>2</sub> and the SST threshold for DTC (Table 7). For 1 × CO<sub>2</sub> levels (355 ppmv), all five AOGCMs indicate a strong relationship between SST and OLR (Fig. 3). OLR generally increases as SST increases until a threshold ocean temperature, above which the OLR values drop considerably (15%–25%), indicative of a sharp increase in DTC activity. These threshold SST values are around 25°C across all AOGCMs (Table 7) and are all warmer than the tropical average SST for the corresponding climate state (vertical lines in Figs. 2–5). This decreasing OLR trend continues until a capping threshold SST is met (around 29°–30°C across all AOGCMs). Here in the warmest SST regions, OLR

values begin to increase once again as large-scale subsidence warms and dries the lower troposphere above the boundary layer (Graham and Barnett 1987; Lau et al. 1997). The relationship between SST and OLR in both future climatic scenarios (2 × CO<sub>2</sub> and 4 × CO<sub>2</sub>) mirrors the SST dependence evident in the current climate; however, the SST thresholds for the corresponding increase and decrease in DTC activity occur at warmer temperatures (Figs. 2 and 3; Table 7). For example, the Geophysical Fluid Dynamics Laboratory Climate Model versions 2.0 and 2.1 (GFDL CM2.0) threshold SST increases from 25°C to 27°C between 1 × CO<sub>2</sub> and 4 × CO<sub>2</sub> (Fig. 2, Table 7), while the more sensitive and higher-resolution AOGCMs (i.e., ECHAM5/MPI-OM) yield amplified SST responses (+5°C) to increased CO<sub>2</sub> concentrations, as expected (Table 7). In contrast to SST, as CO<sub>2</sub> concentrations increase, values of the OLR extremes are relatively stable (Figs. 2 and 3), suggesting little correlation exists between the two. Thus, as CO<sub>2</sub> concentrations increase, the minimum (maximum) SST threshold necessary for DTC initiation (suppression) also increases, but changes in the character of the DTC are not detected. These results are consistent with the observational studies of Graham and Barnett (1987) and WE and with the AOGCM analyses of Dutton et al. (2000), among others.

#### b. PRC versus SST (40°N–40°S)

Utilizing PRC as a proxy for DTC (Figs. 4 and 5) reveals relationships with SST and CO<sub>2</sub> concentrations consistent with the OLR results above. Once again, the threshold SST above which relatively low precipitation

TABLE 5. ECS and TCS values for each AOGCM in Table 1 (Randall et al. 2007).

AOGCM	ECS (°C)	TCS (°C)
GFDL CM2.0	2.9	1.6
GFDL CM2.1	2.9	1.6
ECHAM5/MPI-OM	3.4	2.2
MRI-CGCM2.3.2	3.2	2.2
NCAR PCM	2.1	1.3

TABLE 6. Globally averaged annual mean surface temperature for the three 10-yr bands corresponding to the three reference CO<sub>2</sub> concentrations used here and the 4 × CO<sub>2</sub> – 1 × CO<sub>2</sub> surface temperature difference.

AOGCM	Global-average surface temperature (°C)			Global-average surface temperature increase (°C)
	1 × CO <sub>2</sub>	2 × CO <sub>2</sub>	4 × CO <sub>2</sub>	
GFDL CM2.0	13.8	15.6	16.9	3.1
GFDL CM2.1	14.4	15.8	17.3	2.9
ECHAM5/MPI-OM	15.3	17.9	20.2	4.9
MRI-CGCM2.3.2	14.7	16.7	18.6	3.9
NCAR PCM	13.7	14.9	16.5	2.8

rates begin to increase significantly exceeds the tropical average SST for that climate state. Similarly, as CO<sub>2</sub> concentrations increase, so do the threshold SST ranges for DTC (Table 7, Figs. 4 and 5). Each AOGCM simulates an increase in threshold SST from the 1 × CO<sub>2</sub> to the 4 × CO<sub>2</sub> climate state of between 1.5° and 5.0°C, with the ECHAM5/MPI-OM yielding the highest threshold SST increase and the NCAR PCM simulation yielding the lowest (Fig. 5). The evolving relationship between PRC and SST reported here confirms that a shift in the SST threshold necessary for DTC should be expected in a warmer climate.

### c. PRC versus SST (20°N–20°S)

As discussed above, variations in the monthly averaged PRC over the tropics and subtropics (40°N–40°S) are dominated by activity in the 20°N–20°S band (Fig. 6),

so we now evaluate annually averaged oceanic PRC within this 20°N–20°S tropical band (Table 3). The baseline for comparison is the PRC normalized by model years 1–140 of each AOGCM simulation. The AOGCMs have varied PRC responses to enhanced atmospheric CO<sub>2</sub> concentrations in this region: annually averaged rainfall rates experience little change over time in three of the five AOGCMs (GFDL CM2.0, GFDL CM2.1, and NCAR PCM); however, the two AOGCMs with the highest climate sensitivities (ECHAM5/MPI-OM and MRI-CGCM2.3.2; Table 5) yield between a 12.8% and 13.1% increase in annual rainfall rates across the same region from the first 10 model years to the last 10 model years (Table 3, Fig. 7). Based on these findings, it is clear that the AOGCM climate sensitivities are identifying significant feedback mechanisms that have direct impacts on SST and convective activity within the tropics (Randall et al. 2007).

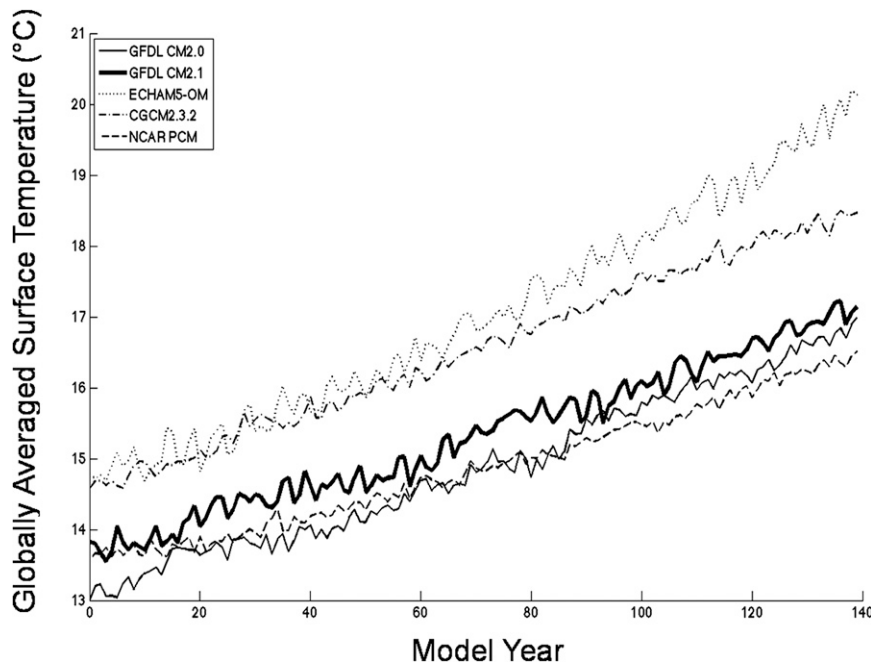


FIG. 1. Annual globally averaged surface temperature across the 140 yr of simulation for each of the AOGCMs listed in Table 1.

TABLE 7. DTC threshold SST bins for each AOGCM for each CO<sub>2</sub> scenario. The threshold temperature was calculated as the SST bin corresponding to the maximum 10-yr mean binned (using a bin of 0.5°C) OLR value for SSTs less than 31°C. For each SST bin, the corresponding SST range is  $\pm 0.25^\circ\text{C}$ .

AOGCM	DTC threshold SST bin ( $^\circ\text{C}$ )			DTC threshold temperature increase ( $^\circ\text{C}$ )
	$1 \times \text{CO}_2$	$2 \times \text{CO}_2$	$4 \times \text{CO}_2$	$(4 \times \text{CO}_2 - 1 \times \text{CO}_2)$
GFDL CM2.0	25.0	26.0	27.0	2.0
GFDL CM2.1	25.0	26.0	27.5	2.5
ECHAM5/MPI-OM	25.0	28.0	30.0	5.0
MRI-CGCM2.3.2	25.0	27.0	28.5	3.5
NCAR PCM	25.0	25.5	26.5	1.5

How does the spatial extent of DTC change with increasing CO<sub>2</sub> concentrations and a warming climate? Following Dutton et al. (2000), we analyze the number of AOGCM grid points per month exceeding established convective threshold values of 12 and 14 mm day<sup>-1</sup> (Table 4). The three AOGCMs that yielded little change in annual rainfall rates also exhibit no trend in spatial extent of these threshold rainfall rates, with 8.7%–13.6% of the tropical oceans having DTC exceeding 12 mm day<sup>-1</sup> and 5.6%–9.5% exceeding 14 mm day<sup>-1</sup> in both the  $1 \times \text{CO}_2$  and  $4 \times \text{CO}_2$  regimes (Table 4). The AOGCMs exhibiting high climate sensitivities and the largest increases in annual rainfall rates (ECHAM5/MPI-OM, MRI-CGCM2.3.2) also display a positive trend

in the spatial extent of DTC exceeding these rain-rate thresholds; the net effect is an increase in the spatial extent of PRC exceeding 12 mm day<sup>-1</sup> (14 mm day<sup>-1</sup>) of 2.3%–6.1% (1.5%–5.2%). Based on these results, increasing levels of CO<sub>2</sub> will either sustain or increase annual convective precipitation rates in the tropics; however, they may—or may not—expand the areal coverage of intense tropical rainfall.

#### 4. Discussion and conclusions

The relationship between tropical convection and SST over the global tropics and subtropics (oceanic locations 40°N–40°S) has been explored for one of the transient

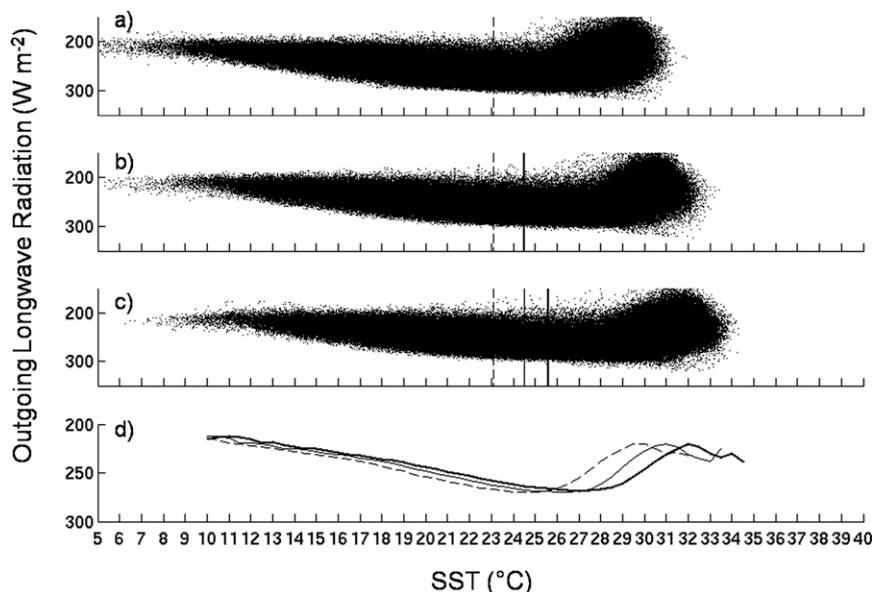


FIG. 2. Distribution of collocated, monthly averaged tropical SST ( $^\circ\text{C}$ ) and OLR ( $\text{W m}^{-2}$ ) across select model 10-yr bands (22–31, 91–100, 140–149) depicting atmospheric CO<sub>2</sub> concentrations of (a)  $1 \times \text{CO}_2$ , (b)  $2 \times \text{CO}_2$ , and (c)  $4 \times \text{CO}_2$  for the GFDL CM2.0. Vertical lines denote the 10-yr-averaged SSTs over 40°N–40°S for the  $1 \times \text{CO}_2$  (dashed),  $2 \times \text{CO}_2$  (thin solid), and  $4 \times \text{CO}_2$  (thick solid) scenarios. (d) Mean values of the same OLR data binned by 0.5°C SST increments are plotted for  $1 \times \text{CO}_2$  (dashed),  $2 \times \text{CO}_2$  (thin solid), and  $4 \times \text{CO}_2$  (thick solid). In all panels, values of OLR decrease upward so that “high” values correspond to more active DTC.

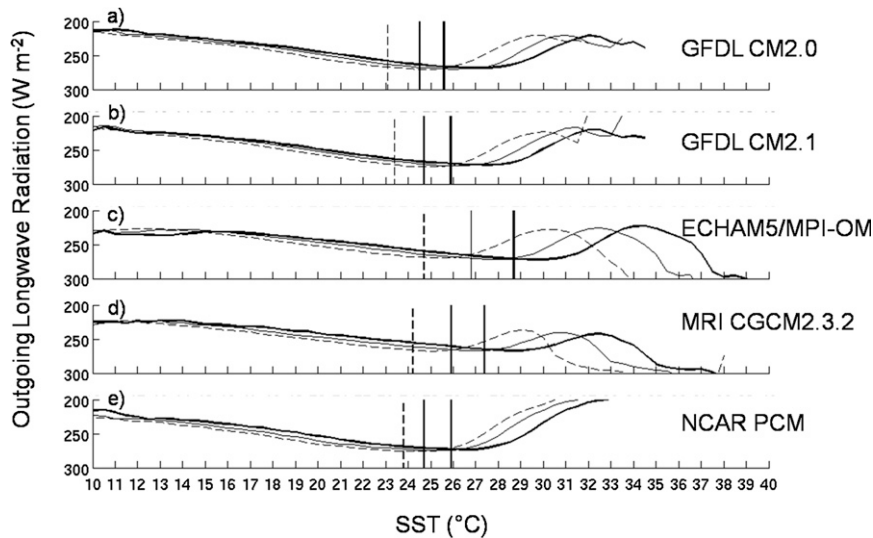


FIG. 3. Mean monthly averaged OLR ( $\text{W m}^{-2}$ ) binned in increments of  $0.5^{\circ}\text{C}$  monthly averaged SST (collocated) across model 10-yr bands depicting atmospheric  $\text{CO}_2$  concentrations of  $1 \times \text{CO}_2$  (dashed),  $2 \times \text{CO}_2$  (thin solid), and  $4 \times \text{CO}_2$  (thick solid) for (a) GFDL CM2.0, (b) GFDL CM2.1, (c) ECHAM5/MPI-OM, (d) MRI-CGCM2.3.2, and (e) NCAR PCM. As in Fig. 2, values of OLR decrease upward in all panels so that high values correspond to more active DTC and the vertical lines denote the 10-yr-averaged SST over  $40^{\circ}\text{N}$ – $40^{\circ}\text{S}$  for  $1 \times \text{CO}_2$  (dashed),  $2 \times \text{CO}_2$  (thin solid), and  $4 \times \text{CO}_2$  (thick solid).

$\text{CO}_2$  forcing experiments (1% annual  $\text{CO}_2$  increase to  $4 \times \text{CO}_2$ , experiment 1PCTTO4X) described in the most recent IPCC assessment (Randall et al. 2007). Five AOGCMs are analyzed for  $1 \times$ ,  $2 \times$ , and  $4 \times \text{CO}_2$  scenarios. Monthly averaged OLR and PRC are used as proxies for deep convection activity. These diagnostics yield consistent results in representing the area-averaged and monthly averaged relationships between DTC and SST, but differ when the spatial extent of intense convection is analyzed.

Simulated OLR and PRC variations with SST indicate a  $25^{\circ}\text{C}$  lower SST bound required for DTC to occur (Table 7). This result is consistent with both observational (Graham and Barnett 1987; Lau et al. 1997) and previous AOGCM/GCM studies (Dutton et al. 2000; Folkins and Braun 2003) of tropical convection variations with SST. This SST threshold is in good agreement with the lower bound for tropical cyclogenesis diagnosed by many investigators (e.g., Miller 1958; Gray 1979; Evans 1993).

Analyses of the five AOGCMs are consistent: this  $1 \times \text{CO}_2$  SST threshold for DTC is not robust to climate change. Increasing atmospheric  $\text{CO}_2$  concentrations correspond to an increase in the tropically averaged SST and result in an increase in this SST threshold for DTC. SST thresholds for DTC increase to  $25.5^{\circ}$ – $28^{\circ}\text{C}$  for  $\text{CO}_2$  doubling and  $26.5^{\circ}$ – $30^{\circ}\text{C}$  for a quadrupling of  $\text{CO}_2$  (Table 7; see also Dutton et al. 2000; Williams

et al. 2009). Equilibrium and transient climate sensitivities track the amplitude of the changing response of OLR and PRC to SST for these climate scenarios: the ECHAM5/MPI-OM and MRI-CGCM2.3.2 AOGCMs have the highest climate sensitivities (Table 5) and also yield the largest increases in SST threshold ( $3.5^{\circ}$ – $5^{\circ}\text{C}$ ) for both OLR and PRC (Table 7), while the three low-sensitivity AOGCMs show only a weak response of the SST threshold ( $1.5^{\circ}$ – $2.5^{\circ}\text{C}$ ) for OLR (Fig. 3) and a somewhat stronger sensitivity to PRC (Fig. 5).

Results from an assessment of changes in the annual and monthly convective rainfall rates with changing atmospheric  $\text{CO}_2$  are driven by climate sensitivity metrics. As  $\text{CO}_2$  concentrations increase by  $1\% \text{ yr}^{-1}$ , annual tropical PRC increases by over 12% for the two high-sensitivity AOGCMs but exhibits little to no change for the other three AOGCM (Figs. 6 and 7, Table 3).

Finally, changes in the spatial extent of the tropical regions experiencing monthly averaged threshold precipitation rates exceeding  $12$  and  $14 \text{ mm day}^{-1}$  are examined (Figs. 8a and 8b, Table 4). Across all five AOGCMs, a quadrupling of  $\text{CO}_2$  concentrations yields only a  $0.49\%$ – $6.1\%$  increase in the spatial extent of these PRC regimes in the latitude band  $20^{\circ}\text{N}$ – $20^{\circ}\text{S}$  (Figs. 8a and 8b). These results are consistent with Dutton et al. (2000) and Trenberth (2011), which suggests that although enhanced atmospheric  $\text{CO}_2$  concentrations effectively

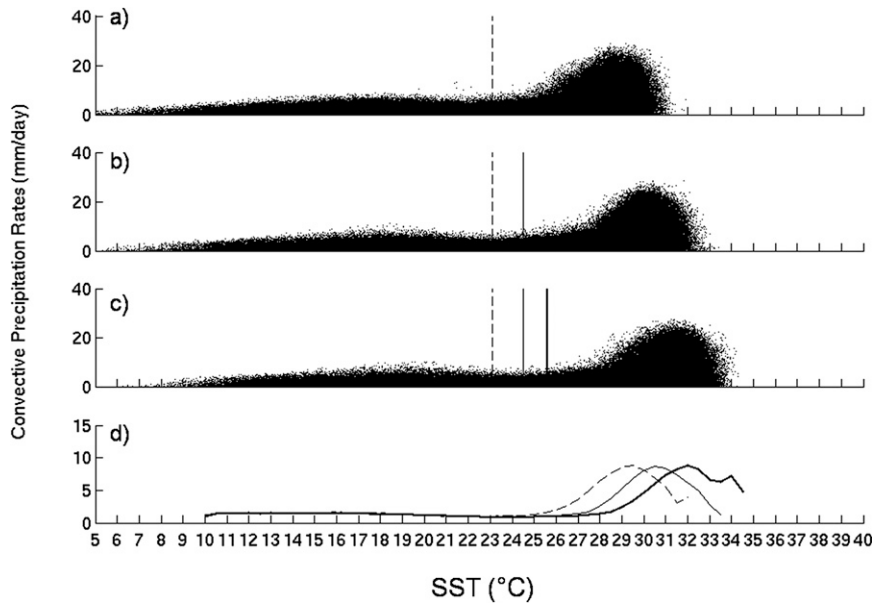


FIG. 4. Distribution of collocated, monthly averaged tropical SST ( $^{\circ}\text{C}$ ) and PRC ( $\text{mm day}^{-1}$ ) across select model 10-yr bands (22–31, 91–100, 140–149) depicting atmospheric  $\text{CO}_2$  concentrations of (a)  $1 \times \text{CO}_2$ , (b)  $2 \times \text{CO}_2$ , and (c)  $4 \times \text{CO}_2$  for the GFDL CM2.0. Vertical lines denote the 10-yr-averaged SST over  $40^{\circ}\text{N}$ – $40^{\circ}\text{S}$  for the  $1 \times \text{CO}_2$  (dashed),  $2 \times \text{CO}_2$  (thin solid), and  $4 \times \text{CO}_2$  (thick solid) scenarios. (d) Mean values of the same PRC data binned by  $0.5^{\circ}\text{C}$  SST increments are plotted for  $1 \times \text{CO}_2$  (dashed),  $2 \times \text{CO}_2$  (thin solid) and  $4 \times \text{CO}_2$  (thick solid).

increase tropical SST and moisture availability, the regions experiencing DTC will not expand significantly.

Results from this study have important implications for climate change projections of TC activity. Empirical

diagnostics show that TCs most commonly form in regions with SST exceeding the threshold values most favorable for DTC. We demonstrate here that all AOGCMs simulate an increase in threshold SST necessary for DTC

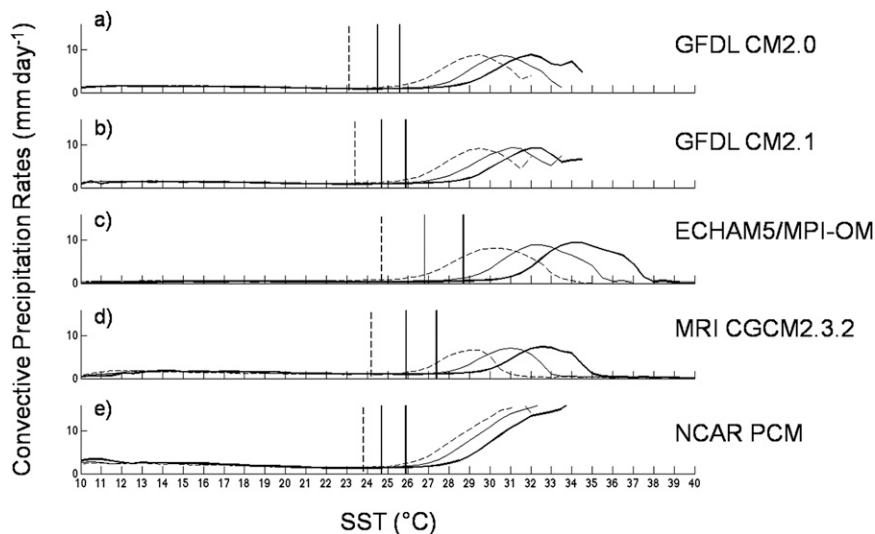


FIG. 5. Mean monthly averaged PRC ( $\text{mm day}^{-1}$ ) binned in increments of  $0.5^{\circ}\text{C}$  monthly averaged SST (collocated) across model 10-yr bands depicting atmospheric  $\text{CO}_2$  concentrations of  $1 \times \text{CO}_2$  (dashed),  $2 \times \text{CO}_2$  (thin solid), and  $4 \times \text{CO}_2$  (thick solid) for (a) GFDL CM2.0, (b) GFDL CM2.1, (c) ECHAM5/MPI-OM, (d) MRI-CGCM2.3.2, and (e) NCAR PCM. As in Fig. 2, the vertical lines denote the 10-yr-averaged SST over  $40^{\circ}\text{N}$ – $40^{\circ}\text{S}$  for  $1 \times \text{CO}_2$  (dashed),  $2 \times \text{CO}_2$  (thin solid), and  $4 \times \text{CO}_2$  (thick solid) scenarios.

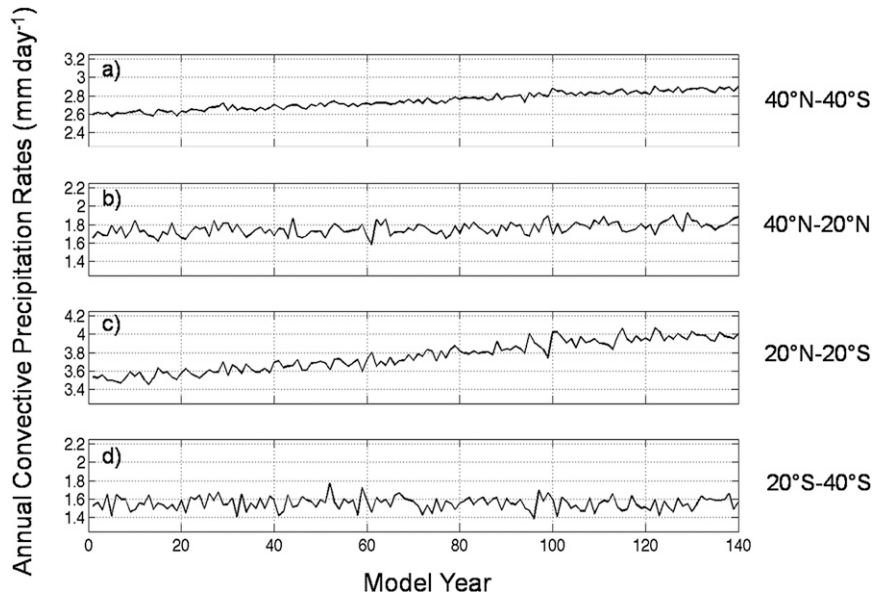


FIG. 6. Annually averaged tropical precipitation rates ( $\text{mm day}^{-1}$ ) from the 140-yr MRI-CGCM2.3.2 simulation for the following regions: (a)  $40^{\circ}\text{N}$ – $40^{\circ}\text{S}$ , (b)  $40^{\circ}\text{N}$ – $20^{\circ}\text{N}$ , (c)  $20^{\circ}\text{N}$ – $20^{\circ}\text{S}$ , and (d)  $20^{\circ}\text{S}$ – $40^{\circ}\text{S}$ .

with increasing globally and tropically averaged surface temperatures. Thus, we conclude that the  $\text{SST} > 26^{\circ}\text{C}$  criterion for tropical cyclogenesis in the  $1 \times \text{CO}_2$  climate (e.g., Miller 1958; Gray 1979) is unlikely to be robust in a changing base climate. Further, these AOGCMs project small increases ( $\sim 0.5\%$ – $6\%$ ) in the areal extent of DTC. This result is consistent with previous studies (e.g., Dutton et al. 2000; Walsh 2004) and argues for a stable spatial domain for tropical cyclogenesis even within a changing base climate.

Factors other than SST should certainly be considered when projecting likely changes of TCs with climate change. The variation of the SST threshold across climate regimes identified here has been argued to be less important than variations in the tropical tropopause temperature in explaining changes in the atmospheric stability (Sobel et al. 2002; Tippett et al. 2011). The potential for a slowing of the mean tropical circulation could be expected to reduce the forcing for DTC (Vecchi and Soden 2007a), consistent with the finding of decreased convective mass flux with global warming (Held and Soden 2006). However, analyses of IPCC AR4 transient  $\text{CO}_2$  simulations of the South Asian summer monsoon (a region favorable for tropical cyclogenesis) show a weakening of the monsoon circulation and increases in monsoon precipitation and latent heating accompanied by increased lower- to mid-troposphere static stability (Fan et al. 2012). Many thermodynamic and dynamic factors (e.g., PV, vertical wind shear) interacting on daily to intraseasonal time scales continuously

modulate the conditions favorable for tropical cyclogenesis (Gray 1979; McBride and Zehr 1981; Vecchi and Soden 2007b; Waters et al. 2012), so it is clear that inferences on tropical cyclogenesis response to SST cannot provide the full picture of TC sensitivity to a changing base climate. Nonetheless, TCs are indisputably intense convective systems, so their variation is necessarily tied to variations in tropical convection.

While theoretical arguments indicate that the potential intensity for tropical cyclones should be expected

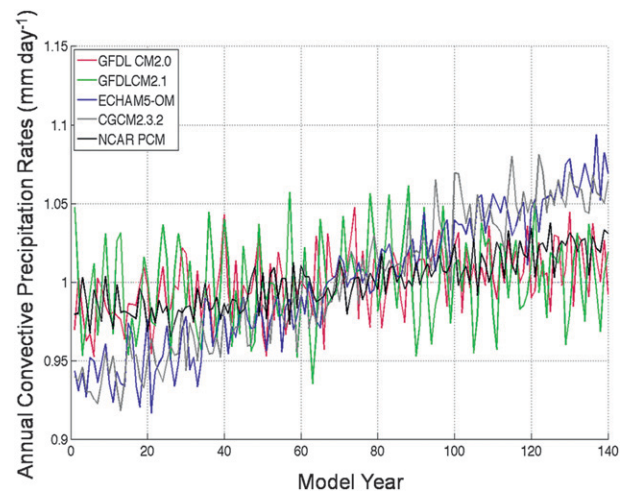


FIG. 7. Annually averaged tropical precipitation rates ( $\text{mm day}^{-1}$ ) normalized (compared to the 1–140-yr average) for the tropical band  $20^{\circ}\text{N}$ – $20^{\circ}\text{S}$  for each AOGCM.

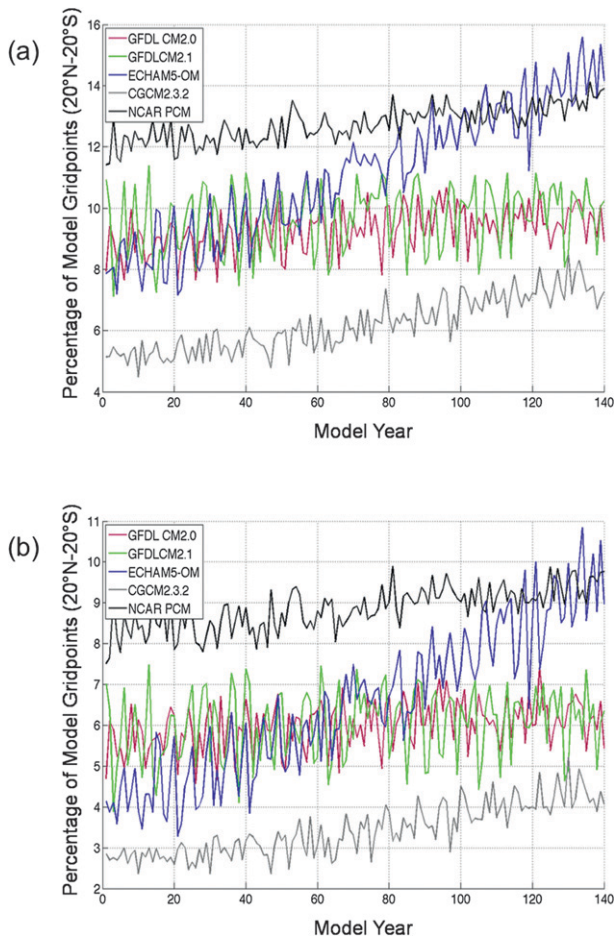


FIG. 8. Percentage of model grid points in the tropical band  $20^{\circ}\text{N}$ – $20^{\circ}\text{S}$  in which the monthly averaged PRC exceed (a) 12 and (b)  $14\text{ mm day}^{-1}$ .

to increase in a warmer climate (e.g., Emanuel 1987; Holland 1997), the small changes in spatial extent of intense precipitation and in average precipitation rates analyzed here do not support changes in the spatial domain for genesis, nor do they argue for large changes in the realized intensity of typical tropical cyclones.

**Acknowledgments.** We first thank Jan Dutton for encouraging us to revisit this problem. We thank Casey Webster for many discussions on these analyses and Holly Hamilton for her assistance with the figures. We are grateful to the individuals from each of the modeling agencies who assisted us in obtaining the GCM runs analyzed here. Chuck Pavloski and Chad Bahrmann provided excellent programming assistance and scientific database management. This work was supported by the National Science Foundation under Grant ATM-0735973.

## REFERENCES

- Bengtsson, L., K. I. Hodges, M. Esch, N. Keenlyside, L. Kornbluh, J. Luo, and T. Yamagata, 2007: How many tropical cyclones change in a warmer climate? *Tellus*, **59**, 539–561.
- Druryan, L., P. Lonergan, and T. Eichler, 1999: A GCM investigation of global warming impacts relevant to tropical cyclone genesis. *Int. J. Climatol.*, **19**, 607–617.
- Dutton, J. F., C. J. Poulsen, and J. L. Evans, 2000: The effect of global climate change on the regions of tropical convection in CSM1. *Geophys. Res. Lett.*, **27**, 3049–3052.
- Emanuel, K. A., 1987: The dependence of hurricane intensity on climate. *Nature*, **326**, 483–485.
- , 1995: Sensitivity of tropical cyclones to surface exchange coefficients and a revised steady-state model incorporating eye dynamics. *J. Atmos. Sci.*, **52**, 3969–3976.
- , 2000: A statistical analysis of tropical cyclone intensity. *Mon. Wea. Rev.*, **128**, 1139–1152.
- , R. Sundararajan, and J. Williams, 2008: Hurricanes and global warming: Results from downscaling IPCC AR4 simulations. *Bull. Amer. Meteor. Soc.*, **89**, 347–367.
- Evans, J. L., 1993: Sensitivity of tropical cyclone intensity to sea surface temperature. *J. Climate*, **6**, 1133–1140.
- , and R. E. Shemo, 1996: A procedure for automated satellite-based identification and climatology development of various classes of organized convection. *J. Appl. Meteor.*, **35**, 638–652.
- , and F. A. Jaskiewicz, 2001: Satellite-based monitoring of intraseasonal variations in tropical Pacific and Atlantic convection. *Geophys. Res. Lett.*, **28**, 1511–1514.
- , B. F. Ryan, and J. L. McGregor, 1994: A numerical exploration of the sensitivity of tropical cyclone rainfall intensity to sea surface temperature. *J. Climate*, **7**, 616–623.
- Fan, F., M. E. Mann, S. Lee and J. L. Evans, 2012: Future changes in the South Asian summer monsoon: Analysis of the CMIP3 multimodel projections. *J. Climate*, **25**, 3909–3928.
- Fierro, A. O., J. Simpson, M. A. LeMone, J. M. Straka, and B. F. Smull, 2009: On how hot towers fuel the Hadley cell: An observational and modeling study of line-organized convection in the equatorial trough from TOGA COARE. *J. Atmos. Sci.*, **66**, 2730–2746.
- Folkens, I., and C. Braun, 2003: Tropical rainfall and boundary layer moist entropy. *J. Climate*, **16**, 1807–1820.
- Gadgil, S., P. V. Joseph, and N. V. Joshi, 1984: Ocean–atmosphere coupling over monsoon regions. *Nature*, **312**, 141–143.
- GFDL, cited 2010a: IPCC DDC AR4 GFDL-CM2.0 1PCTTO4X run1. World Data Center for Climate. [Available online at [http://cera-www.dkrz.de/WDCC/ui/Compact.jsp?acronym=GFDL\\_CM2.0\\_1PCTTO4X\\_1](http://cera-www.dkrz.de/WDCC/ui/Compact.jsp?acronym=GFDL_CM2.0_1PCTTO4X_1)]
- , cited 2010b: IPCC DDC AR4 GFDL-CM2.1 1PCTTO4X run1. World Data Center for Climate. [Available online at [http://cera-www.dkrz.de/WDCC/ui/Compact.jsp?acronym=GFDL\\_CM2.1\\_1PCTTO4X\\_1](http://cera-www.dkrz.de/WDCC/ui/Compact.jsp?acronym=GFDL_CM2.1_1PCTTO4X_1)]
- Graham, N. E., and T. P. Barnett, 1987: Sea surface temperature, surface wind divergence, and convection over tropical oceans. *Science*, **238**, 657–659.
- Gray, W. M., 1968: Global view of the origin of tropical disturbances and storms. *Mon. Wea. Rev.*, **96**, 669–700.
- , 1979: Hurricanes: Their formation, structure and likely role in the tropical circulation. *Meteorology over the Tropical Oceans*, D. B. Shaw, Ed., Royal Meteorological Society, 155–218.
- Gualdi, S., E. Scoccimarro, and A. Navarra, 2008: Changes in tropical cyclone activity due to global warming: Results from

- a high-resolution coupled general circulation model. *J. Climate*, **21**, 5204–5228.
- Held, I. M., and B. J. Soden, 2006: Robust responses of the hydrological cycle to global warming. *J. Climate*, **19**, 5686–5699.
- Holland, G. J., 1997: The maximum potential intensity of tropical cyclones. *J. Atmos. Sci.*, **54**, 2519–2541.
- Lau, K.-M., H. T. Wu, and S. Bony, 1997: The role of large-scale atmospheric circulation in the relationship between tropical convection and sea surface temperature. *J. Climate*, **10**, 381–392.
- , Y. P. Zhou, and H.-T. Wu, 2008: Have tropical cyclones been feeding more extreme rainfall? *J. Geophys. Res.*, **113**, D23113, doi:10.1029/2008JD009963.
- Malkus, J. S., 1963: Cloud patterns over tropical oceans. *Science*, **141**, 767–778.
- McBride, J. L., and R. Zehr, 1981: Observational analysis of tropical cyclone formation. Part II: Comparison of nondeveloping versus developing systems. *J. Atmos. Sci.*, **38**, 1132–1151.
- Miller, B. I., 1958: On the maximum intensity of hurricanes. *J. Meteor.*, **15**, 184–195.
- MRI, cited 2010a: IPCC DDC AR4 MRI-CGCM2.3.2 1PCTTO4X run1. World Data Center for Climate. [Available online at [http://cera-www.dkrz.de/WDCC/ui/Compact.jsp?acronym=MRI\\_CGCM2.3.2\\_1PCTTO4X\\_1](http://cera-www.dkrz.de/WDCC/ui/Compact.jsp?acronym=MRI_CGCM2.3.2_1PCTTO4X_1).]
- , cited 2010b: Experiments for the IPCC-AR4 with MRI CGCM2.3.2. [Available online at <http://www.mri-jma.go.jp/Dep/cl/cl4/IPCC-AR4/simulations.html>.]
- NCAR, cited 2010: IPCC DDC AR4 NCAR-PCM 1PCTTO4X run1. World Data Center for Climate. [Available online at [http://cera-www.dkrz.de/WDCC/ui/Compact.jsp?acronym=NCAR\\_PCM\\_1PCTTO4X\\_1](http://cera-www.dkrz.de/WDCC/ui/Compact.jsp?acronym=NCAR_PCM_1PCTTO4X_1).]
- Oort, A. H., and J. J. Yienger, 1996: Observed interannual variability in the Hadley circulation and its connection to ENSO. *J. Climate*, **9**, 2751–2767.
- Oouchi, K., J. Yoshimura, H. Yoshimura, R. Mizuta, S. Kusunoki, and A. Noda, 2006: Tropical cyclone climatology in a global-warming climate as simulated in a 20 km-mesh global atmospheric model: Frequency and wind intensity analyses. *J. Meteor. Soc. Japan*, **84**, 259–276.
- PCMDI, cited 2010: About the WCRP CMIP3 multi-model dataset archive at PCMDI. [Available online at [http://www.pcmdi.llnl.gov/ipcc/about\\_ipcc.php](http://www.pcmdi.llnl.gov/ipcc/about_ipcc.php).]
- Randall, D. A., and Coauthors, 2007: Climate models and their evaluation. *Climate Change 2007: The Physical Science Basis*, S. D. Solomon et al., Eds., Cambridge University Press, 589–662.
- Roeckner, E., cited 2010: IPCC DDC AR4 ECHAM5/MPI-OM 1PCTTO4X run1. World Data Center for Climate. [Available online at [http://cera-www.dkrz.de/WDCC/ui/Compact.jsp?acronym=EH5\\_MPI\\_OM\\_1PCTTO4X\\_1](http://cera-www.dkrz.de/WDCC/ui/Compact.jsp?acronym=EH5_MPI_OM_1PCTTO4X_1).]
- Royer, J. F., F. Chauvin, B. Timbal, P. Araspin, and D. Grimal, 1998: A GCM study of the impact of greenhouse gas increase on the frequency of occurrence of tropical cyclones. *Climatic Change*, **38**, 307–343.
- Ryan, B. F., I. G. Watterson, and J. L. Evans, 1992: Tropical cyclone frequencies inferred from Gray's yearly genesis parameter: Validation of GCM tropical climates. *Geophys. Res. Lett.*, **19**, 1831–1834.
- Shemo, R. E., and J. L. Evans, 1996: Contributions of various classes of convection to rainfall in the Atlantic Ocean. *Meteor. Atmos. Phys.*, **60**, 191–205, doi:10.1007/BF01029795.
- Sobel, A. H., I. M. Held, and C. S. Bretherton, 2002: The ENSO signal in tropical tropospheric temperature. *J. Climate*, **15**, 2702–2706.
- Sugi, M., H. Murakami, and J. Yoshimura, 2009: A reduction in global tropical cyclone frequency due to global warming. *SOLA*, **5**, 164–167.
- Tippett, M. K., S. J. Camargo, and A. H. Sobel, 2011: A Poisson regression index for tropical cyclone genesis and the role of large-scale vorticity in genesis. *J. Climate*, **24**, 2335–2357.
- Trenberth, K., 2011: Changes in precipitation with climate change. *Climate Res.*, **47**, 123–138, doi:10.3354/cr00953.
- Vecchi, G. A., and B. J. Soden, 2007a: Global warming and the weakening of the tropical circulation. *J. Climate*, **20**, 4316–4340.
- , and —, 2007b: Increased tropical Atlantic wind shear in model projections of global warming. *Geophys. Res. Lett.*, **34**, L08702, doi:10.1029/2006GL028905.
- Walsh, K., 2004: Tropical cyclones and climate change: Unresolved issues. *Climate Res.*, **27**, 77–83.
- Waters, J. J., J. L. Evans, and C. E. Forest, 2012: Large-scale diagnostics of tropical cyclogenesis potential using environment variability metrics and logistic regression models. *J. Climate*, **25**, 6092–6107.
- Williams, I. N., R. T. Pierrehumbert, and M. Huber, 2009: Global warming, convective threshold and false thermostats. *Geophys. Res. Lett.*, **36**, L21805, doi:10.1029/2009GL039849.
- Zhang, C., 1993: Large-scale variability of atmospheric deep convection in relation to sea surface temperature in the tropics. *J. Climate*, **6**, 1898–1913.